Two complementary lattice-Boltzmann-based analyses for nonlinear systems

Hiroshi Otomo, Bruce M. Boghosian

Department of Mathematics, Tufts University, Medford, Massachusetts 02155, USA

François Dubois

CNAM Paris, Laboratoire de mécanique des structures et des systèmes couplés, 292, rue Saint-Martin, 75141 Paris cedex 03,France

Université Paris-Sud, Laboratoire de mathématiques, UMR CNRS 8628, 91405 Orsay cedex, France

Department of Mathematics, University Paris-Sud, Bat. 425, F-91405 Orsay, France

Abstract

Lattice Boltzmann models that asymptotically reproduce solutions of nonlinear systems are derived by the Chapman-Enskog method and the analytic method based on recursive substitution and Taylor-series expansion. While both approaches yield identical hydrodynamic equations and can be generalized to analyze a variety of nonlinear systems, they have complementary advantages and disadvantages. In particular, the error analysis is substantially easier using the Taylor-series expansion method. In this work, the Burgers', Korteweg-de Vries, and Kuramoto-Sivashinsky equations are analyzed using both approaches, and the results are discussed and compared with analytic solutions and previous studies.

Keywords: `Lattice Boltzmann equation, Chapman-Enskog analysis, Burgers equation, Korteweg-de Vries equation, Kuramoto-Sivashinsky equation`

Contents

1. Introduction

The lattice Boltzmann (LB) equation is a discrete hydrodynamic model, based on an underlying discrete-velocity kinetic equation [1]. It implements fundamental processes, particle propagation and collisional relaxation, which can be tuned to reproduce various macroscopic physical phenomena. Specifically the formalism is motivated by an asymptotic analysis of the Boltzmann equation.

To relate the microscopic LB transport equation to the macroscopic hydrodynamic equations, a commonly used analytic method is the Chapman-Enskog method. Using the Knudsen number, which is the assumedly small ratio of the mean free path to the macroscopic length scale, as an expansion parameter,

Email address: `hiroshi.otomo@tufts.edu` (Hiroshi Otomo)

the LB equation is expanded order by order. For mass- and momentum-conserving LB models, it is well known that the expansion up to the second order yields the continuity equation and the Navier-Stokes equation. Indeed, this is one of basic motivations for extensive applications of the LB method in the computational fluid dynamics field.

In this paper, for simulating more general nonlinear equations we proceed to the Burnett level – up to the fourth derivative order. In previous studies [2–7], reasonably accurate LB models are derived by the Chapman-Enskog method for a variety of nonlinear systems. In most of their studies, however, they have found it necessary to introduce a correction term to the BGK collision operator, called the *amending function*, whose physical meaning is not entirely clear. In this paper, we demonstrate that, by introducing scaling parameters in the functional form of the local equilibrium, LB models with similar or greater accuracy can be constructed with no amending function.

An alternative analysis expands the LB equation in a Taylor series, supposing that $\Delta x\,\partial_x$ is of order ϵ, and $\Delta t\,\partial_t$ is of order ϵ^m where $m \geq 1$ and ϵ is a tiny parameter [8–10]. Because the macroscopic equation is derived by straightforward algebra from the LB equation, this method is well suited for error analysis [8] and the analysis of complex fluids, such as multiphase flow [9, 11].

In this work, both of the above-described analytic methods are applied to derive LB models corresponding to various nonlinear equations in $1+1$ dimensions. Moreover, features of each method are discussed and, using the models thus derived, several nonlinear systems are simulated, including the Burgers', Korteweg-de Vries (KdV), and Kuramoto-Sivashinsky (KS) equations.

For space x and time t, the Burgers' equation is

$$\partial_t \rho + \rho \partial_x \rho = \partial_x^2 \rho, \tag{1}$$

the KdV equation is

$$\partial_t \rho - 6\rho \partial_x \rho = -\partial_x^3 \rho, \tag{2}$$

and the KS equation is

$$\partial_t \rho + \rho \partial_x \rho = -\partial_x^2 \rho - \partial_x^4 \rho. \tag{3}$$

In all three cases, the second term on the left-hand side is regarded as the advection term and the terms on the right hand side are diffusion, anti-diffusion or hyperdiffusion terms.

The KS equation has been applied to a variety of chaotic phenomena such as the flame front in laminar flow of burning gas [12, 13], and the thickness of a thin-water film on a vertical wall [14]. Indeed, Holmes [15] has observed that similar terms can be found in the equations for turbulent fluctuation velocity derived from the Navier-Stokes equation. Hence, study of the KS equation helps to deepen our knowledge of turbulence.

The outline of this paper is as follows: In Sec. 2, the LB method for nonlinear equations is formulated using both the Chapman-Enskog method and the Taylor expansion method. In Sec. 3, the LB models thus obtained are tested by comparison with analytical solutions and previous study. In Sec. 4, the results obtained by this study are summarized and discussed.

2. Lattice Boltzmann models for the nonlinear system

The LB equation for the discrete distribution function f_i is given by:

$$f_i\left(x + c_i\Delta t, t + \Delta t\right) - f_i\left(x, t\right) = -\frac{f_i\left(x, t\right) - f_i^{eq}\left(x, t\right)}{\tau}, \tag{4}$$

where c_i is the discrete lattice velocity and τ is the relaxation time. Here, f_i^{eq} denotes the local equilibrium state. For convenience in the Taylor expansion method, by redefining x and t properly, this equation can be recast as,

$$f_i\left(x, t\right) - f_i\left(x - c_i\Delta t, t - \Delta t\right) = -\frac{f_i\left(x - c_i\Delta t, t - \Delta t\right) - f_i^{eq}\left(x - c_i\Delta t, t - \Delta t\right)}{\tau}. \tag{5}$$

The characteristic lattice speed $|c|$, which is dimensioned in lattice units, is assumed to be one and not explicitly written in what follows.

After rearrangement, Eq. (5) can be written in the form,

$$f_i\left(x, t\right) = f_i^{eq}\left(x - c_i\Delta t, t - \Delta t\right) + \left(1 - \frac{1}{\tau}\right)\left\{f_i\left(x - c_i\Delta t, t - \Delta t\right) - f_i^{eq}\left(x - c_i\Delta t, t - \Delta t\right)\right\}. \tag{6}$$

The first term on the right-hand side is the equilibrium distribution, and the second term includes the various non-equilibrium contributions to the distribution.

A macroscopic quantity ρ is defined to be the sum of f_i for states i, $\rho = \sum_i f_i$, and we suppose that it is the only conserved density in the problem. In what follows, we discuss the correspondence between the LB equation, Eq. (6), and the nonlinear equation governing ρ on the basis of two methods. The main goal is to find the form of f_i^{eq} so as to obtain the desired nonlinear equation.

2.1. Derivation with the Chapman-Enskog method

In the Chapman-Enskog method, the Boltzmann equation is expanded by a non-dimensional small parameter ϵ, which is usually regarded as a ratio between microscopic and macroscopic scales, and hence related to the Knudsen number. We choose a local equilibrium distribution of the form,

$$f_i^{eq}(\rho) = W_{i,0} r(\rho) + W_{i,1} c_i p(\rho) + W_{i,2} \left(c_i^2 - c_{S,2}^2\right) g(\rho) + W_{i,3} c_i^3 h(\rho) + W_{i,4} \left(c_i^4 - c_{T,4}^4\right) q(\rho). \tag{7}$$

For maximum generality, we have employed families of weights, $W_{j,a}$, chosen to satisfy

$$\begin{array}{lllll} \sum_i W_{i,a} = 1, & \sum_i W_{i,a} c_i = 0, & \sum_i W_{i,a} c_i^2 = c_{S,a}^2, & \sum_i W_{i,a} c_i^3 = 0, & \sum_i W_{i,a} c_i^4 = c_{T,a}^4, \\ \sum_i W_{i,a} c_i^5 = 0, & \sum_i W_{i,a} c_i^6 = c_{U,a}^6, & \sum_i W_{i,a} c_i^7 = 0, & \sum_i W_{i,a} c_i^8 = c_{V,a}^8, & \sum_i W_{i,a} c_i^9 = 0, \end{array} \tag{8}$$

where $c_{S,a}/c_{T,a}$ are a sound/thermal speed and $c_{U,a}$ and $c_{V,a}$ are two other speeds for each family of weights $W_{i,a}$. Moreover, the functions r, p, g, h, and q in Eq. (7) are expanded by ϵ,

$$r = \sum_{l=0}^{\infty} \epsilon^l r_l(\rho), \quad p = \sum_{l=0}^{\infty} \epsilon^l p_l(\rho), \quad g = \sum_{l=0}^{\infty} \epsilon^l g_l(\rho), \quad h = \sum_{l=0}^{\infty} \epsilon^l h_l(\rho), \quad q = \sum_{l=0}^{\infty} \epsilon^l q_l(\rho). \tag{9}$$

Accordingly the equilibrium state f_i^{eq} is written in the expanded form,

$$f_i^{eq}(\rho) = \sum_{l=0}^{\infty} \epsilon^l f_i^{(eq,l)}(\rho). \tag{10}$$

That is, as noted in the Introduction, the equilibrium state itself varys as the scaling limit is approached.

Although from Eq. (7) it is straightforward to compute the first four moments, for simplicity instead of writing those explicit forms we briefly define following functions of ρ,

$$Q_l = \sum_i f_i^{(eq,l)}, \quad J_l = \sum_i f_i^{(eq,l)} c_i, \quad K_l = \sum_i f_i^{(eq,l)} c_i^2, \quad L_l = \sum_i f_i^{(eq,l)} c_i^3, \quad M_l = \sum_i f_i^{(eq,l)} c_i^4. \tag{11}$$

Because $Q_l(\rho) = r_l(\rho)$ and $r_0(\rho) = \rho$, the r_j for $j > 0$ would break the conservation of ρ via the collision process. For the modeling of hydrodynamic equations with source or sink terms, those terms are useful. In this paper we consider only hydrodynamics with conserved ρ, and therefore we take $r_j = 0$ for $j > 0$. Moreover we assume the differentiability of ρ throughout this analysis.

From Eq. (6), one obtains

$$f_i(x,t) = \left[1 + \tau \left(e^{D_i} - 1\right)\right]^{-1} f_i^{eq}(x,t), \tag{12}$$

where D_i is the differential operator

$$D_i = \partial_t + c_i \partial_x. \tag{13}$$

In terms of ϵ, time and space are scaled so that $\partial_t = \sum_{k=1}^{\infty} \epsilon^k \partial_{t_k}$ and $\partial_x = \epsilon \partial_{x_1}$, where x_k and t_k denote the kth space and time scale [16]. Then D_i is expanded,

$$D_i = \sum_{k=1}^{\infty} \epsilon^k D_{i,k}, \tag{14}$$

where $D_{i,k} := \partial_{t_k} + \delta_{k,1} c_i \partial_{x_1}$ and δ is the Kronecker delta. Consequently the solution of Eq. (12) is

$$f_i(x,t) = \sum_{k=0}^{\infty} \epsilon^k f_i^{(k)}(x,t), \tag{15}$$

where

$$
\begin{aligned}
f_i^{(0)}(x,t) &= f_i^{(eq,0)}, && \text{(16a)}\\
f_i^{(1)}(x,t) &= -\tau D_{i,1} f_i^{(eq,0)} + f_i^{(eq,1)}, && \text{(16b)}\\
f_i^{(2)}(x,t) &= -\tau \left[D_{i,2} - \left(\tau - \tfrac{1}{2}\right) D_{i,1}^2 \right] f_i^{(eq,0)} - \tau D_{i,1} f_i^{(eq,1)} + f_i^{(eq,2)}, && \text{(16c)}\\
f_i^{(3)}(x,t) &= -\tau \left[D_{i,3} - 2\left(\tau - \tfrac{1}{2}\right) D_{i,1} D_{i,2} + \left(\tau^2 - \tau + \tfrac{1}{6}\right) D_{i,1}^3 \right] f_i^{(eq,0)} \\
&\quad -\tau \left[D_{i,2} - \left(\tau - \tfrac{1}{2}\right) D_{i,1}^2 \right] f_i^{(eq,1)} - \tau D_{i,1} f_i^{(eq,2)} + f_i^{(eq,3)}, && \text{(16d)}\\
f_i^{(4)}(x,t) &= -\tau \Big[D_{i,4} - 2\left(\tau - \tfrac{1}{2}\right) D_{i,1} D_{i,3} - \left(\tau - \tfrac{1}{2}\right) D_{i,2}^2 \\
&\qquad + 3\left(\tau^2 - \tau + \tfrac{1}{6}\right) D_{i,1}^2 D_{i,2} - \left(\tau - \tfrac{1}{2}\right)\left(\tau^2 - \tau + \tfrac{1}{12}\right) D_{i,1}^4 \Big] f_i^{(eq,0)} \\
&\quad -\tau \left[D_{i,3} - 2\left(\tau - \tfrac{1}{2}\right) D_{i,1} D_{i,2} + \left(\tau^2 - \tau + \tfrac{1}{6}\right) D_{i,1}^3 \right] f_i^{(eq,1)} \\
&\quad -\tau \left[D_{i,2} - \left(\tau - \tfrac{1}{2}\right) D_{i,1}^2 \right] f_i^{(eq,2)} - \tau D_{i,1} f_i^{(eq,3)} + f_i^{(eq,4)}. && \text{(16e)}
\end{aligned}
$$

If one takes the sum over i in those equations, demanding that the zeroth moments of $f_i^{(l)}$ vanish for $l > 0$, a set of macroscopic equations is obtained for each order in ϵ. The results are summarized in Table 1. In derivation processes of the kth order, we assume suppression of lower-order motions by demanding $\partial_{t_j}\rho = 0$ for $j < k$. Finally, the moments in Eq. (11) are chosen so that the nonlinear equations of interest – the Burgers', KdV, and KS equations – are obtained at the order in ϵ corresponding to the order of the differential equation.

Table 1: Equations of motion and suppression conditions for each order in ϵ

ϵ order	Equations of motion		Conditions for $\partial_{t_i}\rho = 0$	
1	$\partial_{t_1}\rho + J_0'\partial_{x_1}\rho = 0$	(17)	$J_0' = 0$	(18)
2	$\partial_{t_2}\rho = \partial_{x_1}\left\{\left(\tau - \frac{1}{2}\right) K_0' \partial_{x_1}\rho\right\} - J_1'\partial_{x_1}\rho.$	(19)	$K_0' = 0, \quad J_1' = 0,$	(20)
3	$\partial_{t_3}\rho = -\partial_{x_1}^2\left\{\left(\tau^2 - \tau + \frac{1}{6}\right) L_0' \partial_{x_1}\rho\right\} + \left(\tau - \frac{1}{2}\right)\left(K_1''\left(\partial_{x_1}\rho\right)^2 + K_1'\partial_{x_1}^2\rho\right) - J_2'\partial_{x_1}\rho.$	(21)	$L_0' = 0, \quad K_1' = 0, \quad J_2' = 0,$	(22)
4	$\partial_{t_4}\rho = \left(\tau - \frac{1}{2}\right)\left(\tau^2 - \tau + \frac{1}{12}\right)\partial_{x_1}^4 M_0 - \left(\tau^2 - \tau + \frac{1}{6}\right)\partial_{x_1}^3 L_1 + \left(\tau - \frac{1}{2}\right)\partial_{x_1}^2 K_2 - \partial_{x_1} J_3$	(23)	-	

Burgers' equation has second-order spatial derivatives, and therefore requires use of this formalism up to order ϵ^2, i.e., Eq. (19). To make the result equivalent to Burgers' equation, Eq. (1), we see that we should choose,

$$J_1 = \rho^2/2, \;\; K_0 = \rho/\left(\tau - 1/2\right), \tag{24}$$

keeping in mind the requirement for the suppression of first-order motion, Eq. (18) in Table 1.

The KdV equation, Eq. (2), has third-order spatial derivatives, and therefore requires use of this formalism up to order ϵ^3; i.e., Eq. (21). To make the result equivalent to the KdV equation, we see that we should choose,

$$J_2 = -3\rho^2, \;\; K_1 = 0, \;\; L_0 = \rho/\left(\tau^2 - \tau + \tfrac{1}{6}\right), \tag{25}$$

keeping in mind the requirements for the suppression of first and second order motion, Eqs. (18) and (20) in Table 1.

The KS equation, Eq. (3), has fourth-order spatial derivatives, and therefore requires use of this formalism up to order ϵ^4, i.e., Eq. (23). To make the result equivalent to the KS equation, we see that we should choose,

$$J_3 = \rho^2/2, \;\; K_2 = -\rho/\left(\tau - 1/2\right), \;\; L_1 = 0, \;\; M_0 = -\rho/\left\{\left(\tau - 1/2\right)\left(\tau^2 - \tau + 1/12\right)\right\}, \tag{26}$$

keeping in mind the requirements for the suppression of first, second, and third order motion, given in Eqns. (18), (20) and (22), respectively, in Table 1.

2.2. Derivation with the Taylor-expansion method

In this method, after applying a Taylor expansion to the LB equation, higher-order derivative terms of ρ are assumed to be negligible, in the sense that $\Delta x\,\partial_x$ is of order ϵ, and $\Delta t\,\partial_t$ is of order ϵ^m where $m \geq 1$ and ϵ is a tiny parameter. Here, we suppose that $\Delta x/L = \epsilon$ and $\Delta t/T = \epsilon^m$ while $L\partial_x$ and $T\partial_t$ are unity order where L and T are macroscpic length and time.

After the form of f_i in Eq (6) is recursively substituted [1] for f_i on the right-hand side of Eq. (6), the equation is closed with the equilibrium state,

$$\begin{aligned} f_i(x,t) &= f_i^{eq}(x - c_i\Delta t, t - \Delta t) \\ &\quad + \sum_{n=1}^{\infty}\left(1 - \frac{1}{\tau}\right)^n \left\{f_i^{eq}(x - (n+1)c_i\Delta t, t - (n+1)\Delta t) - f_i^{eq}(x - nc_i\Delta t, t - n\Delta t)\right\}. \end{aligned} \tag{27}$$

Here we assume f_i^{eq} has a form,

$$f_i^{eq} = \rho w_i^{(1)} + \rho w_i^{(2)} + \rho w_i^{(3)} + \rho^2 w_i^{(4)}, \tag{28}$$

with weights w_i whose moments are shown in Table 2. The equilibrium distribution, f_i^{eq} should be an analytic function.

Table 2: Moments of w_i in Eq. (28)

Order of moment	$w_i^{(1)}$	$w_i^{(2)}$	$w_i^{(3)}$	$w_i^{(4)}$
0	1	0	0	0
1	0	0	0	$\mathcal{J}$
2	0	0	$\mathcal{K}$	0
3	0	$\mathcal{L}$	0	0
4	$\mathcal{M}$	0	0	0

In Eq.(27) one takes the sum for i. It is readily seen that the left hand side is $\rho(x,t)$. The equilibrium part in the right hand side becomes,

$$\begin{aligned} &\sum_i f_i^{eq}(x - c_i\Delta t, t - \Delta t) \\ &= \sum_i \sum_{m=0}^{\infty} \frac{(-\Delta t)^m}{m!}\left(\frac{\partial}{\partial t} + \left(c_i \cdot \frac{\partial}{\partial x}\right)\right)^m f_i^{eq}(x,t) \\ &= \rho - \Delta t\left(\frac{\partial \rho}{\partial t} + \mathcal{J}\frac{\partial \rho^2}{\partial x}\right) + \frac{\mathcal{K}}{2!}(\Delta t)^2 \frac{\partial^2 \rho}{\partial x^2} - \frac{\mathcal{L}}{3!}(\Delta t)^3 \frac{\partial^3 \rho}{\partial x^3} + \frac{\mathcal{M}}{4!}(\Delta t)^4 \frac{\partial^4 \rho}{\partial x^4} + \mathcal{O}\left(\frac{\partial^5 \rho}{\partial x^5}, \frac{\partial^2 \rho^2}{\partial x \partial t}, \frac{\partial^2 \rho}{\partial t^2}\right). \end{aligned} \tag{29}$$

Similarly, for the non-equilibrium part of Eq. (27), we get

$$\begin{aligned} &\sum_i \sum_{n=1}^{\infty}\left(1 - \frac{1}{\tau}\right)^n \left\{f_i^{eq}(x - (n+1)c_i\Delta t, t - (n+1)\Delta t) - f_i^{eq}(x - nc_i\Delta t, t - n\Delta t)\right\} \\ &= -\Delta t \mathcal{T}_1\left(\frac{\partial \rho}{\partial t} + \mathcal{J}\frac{\partial \rho^2}{\partial x}\right) + \frac{\mathcal{K}}{2!}(\Delta t)^2 \frac{\partial^2 \rho}{\partial x^2}\mathcal{T}_2 - \frac{\mathcal{L}}{3!}(\Delta t)^3 \frac{\partial^3 \rho}{\partial x^3}\mathcal{T}_3 + \frac{\mathcal{M}}{4!}(\Delta t)^4 \frac{\partial^4 \rho}{\partial x^4}\mathcal{T}_4 + \mathcal{O}\left(\frac{\partial^5 \rho}{\partial x^5}, \frac{\partial^2 \rho^2}{\partial x \partial t}, \frac{\partial^2 \rho}{\partial t^2}\right), \end{aligned} \tag{30}$$

where $\mathcal{T}_i = \sum_{n=1}^{\infty}\left(1 - \frac{1}{\tau}\right)^n \left[(n+1)^i - n^i\right]$ whose explicit forms for $\tau > 1/2$ are,

$$\mathcal{T}_1 = \tau - 1,\ \mathcal{T}_2 = 2\tau^2 - \tau - 1,\ \mathcal{T}_3 = 6\tau^3 - 6\tau^2 + \tau - 1,\ \mathcal{T}_4 = H(\tau) - 1, \tag{31}$$

[1] In this recursive substitution, we assume that the domain is infinite, so we do not need to worry about the effect of boundaries.

where $H(\tau) = (\tau - 1)\left(24\tau^3 - 12\tau^2 + 2\tau + 1\right) + 1$. As a result, from Eq. (27) we obtain,

$$\frac{\partial \rho}{\partial t} = -\mathcal{J}\frac{\partial \rho^2}{\partial x} + \frac{\Delta t}{2!}\mathcal{K}\frac{\partial^2 \rho}{\partial x^2}\frac{\mathcal{T}_2 + 1}{\mathcal{T}_1 + 1} - \frac{(\Delta t)^2}{3!}\mathcal{L}\frac{\partial^3 \rho}{\partial x^3}\frac{\mathcal{T}_3 + 1}{\mathcal{T}_1 + 1} + \frac{(\Delta t)^3}{4!}\mathcal{M}\frac{\partial^4 \rho}{\partial x^4}\frac{\mathcal{T}_4 + 1}{\mathcal{T}_1 + 1} + \mathcal{O}\left(\frac{\partial^5 \rho}{\partial x^5}, \frac{\partial^2 \rho^2}{\partial x \partial t}, \frac{\partial^2 \rho}{\partial t^2}\right). \quad (32)$$

Next, we consider the correspondence between Eq. (32) and the desired nonlinear equations for $\tau > 1/2$. For the Burgers' equation, the moments should be set as

$$\mathcal{J} = 1/2,\ \ \mathcal{K} = 1/(\tau - 1/2),\ \ \mathcal{L} = 0,\ \ \mathcal{M} = 0. \quad (33)$$

For the KdV equation, the required moments are

$$\mathcal{J} = -3,\ \ \mathcal{K} = 0,\ \ \mathcal{L} = 1/\left(\tau^2 - \tau + 1/6\right),\ \ \mathcal{M} = 0. \quad (34)$$

For the KS equation, the moments should be set as

$$\mathcal{J} = 1/2,\ \ \mathcal{K} = -1/(\tau - 1/2),\ \ \mathcal{L} = 0,\ \ \mathcal{M} = -1/\left[(\tau - 1/2)\left(\tau^2 - \tau + 1/12\right)\right]. \quad (35)$$

2.3. Summary of formalism

If x and t denote the space and time coordinates in lattice units, as used in the simulation, then the physical space X and time T are defined as

$$\begin{aligned} X &= \alpha x \\ T &= \beta t, \end{aligned} \quad (36)$$

where α and β are scaling parameters. From a physical viewpoint, such scaling is sometimes necessary to enhance the accuracy and stability of the simulation. From a mathematical viewpoint, it can be used to reduce the effects of truncation error of the higher-order space and time derivatives.

As is evident from comparing Eqs. (24) and (33), Eqs. (25) and (34), and Eqs. (26) and (35), respectively, for each nonlinear equation, both analytic methods yield the same results. That is, for solving nonlinear equations, Eq.(6) is solved using f_i^{eq} described in Eq. (28), Table 2, and Table 3. These analytic methods are very different and it is not at all clear that they should give the same numerical algorithm, but one of the principal results of this paper is that they do so for all three of hydrodynamic equations.

Table 3: Moments for each nonlinear equation

	Burgers'	KdV	KS
$\mathcal{J}$	$\beta/2\alpha$	$-3\beta/\alpha$	$\beta/2\alpha$
$\mathcal{K}$	$\beta/\left\{\alpha^2(\tau - 1/2)\right\}$	0	$-\beta/\left\{\alpha^2(\tau - 1/2)\right\}$
$\mathcal{L}$	0	$\beta/\left\{\alpha^3\left(\tau^2 - \tau + 1/6\right)\right\}$	0
$\mathcal{M}$	0	0	$-\beta/\left\{\alpha^4(\tau - 1/2)\left(\tau^2 - \tau + 1/12\right)\right\}$

Henceforth, we adopt notation that has become standard in the lattice Boltzmann literature, in which $DnQm$ refers to a model in n spatial dimensions with m kinetic velocities. In the case of D1Q5, for which $c_i = \{0, \pm 1, \pm 2\}$, if we demand that the moments are as listed Table 2, then the w_i must be

$$\begin{aligned} w_i^{(1)} = \mathcal{M}\{1/4 + 1/\mathcal{M}, -1/6, 1/24\}, w_i^{(2)} = \mathcal{L}\{0, \mp 1/6, \pm 1/12\}, \\ w_i^{(3)} = \mathcal{K}\{-5/4, 2/3, -1/24\}, w_i^{(4)} = \mathcal{J}\{0, \pm 2/3, \mp 1/12\}. \end{aligned} \quad (37)$$

For D1Q7, for which $c_i = \{0, \pm 1, \pm 2 \pm 3\}$, if we demand that the first four moments are as listed Table 2 and the fifth and sixth moments vanish, then the w_i must be

$$\begin{aligned} w_i^{(1)} = \mathcal{M}\{7/18 + 1/\mathcal{M}, -13/48, 1/12, -1/144\},\ \ w_i^{(2)} = \mathcal{L}\{0, \mp 13/48, \pm 1/6 \mp 1/48\}, \\ w_i^{(3)} = \mathcal{K}\{-49/36, 3/4, -3/40, 1/180\},\ \ w_i^{(4)} = \mathcal{J}\{0, \pm 3/4, \mp 3/20, \pm 1/60\}. \end{aligned} \quad (38)$$

The above lattice vectors and weights are utilized in the next section.

It is worth noting that all of the conserved quantities in the original nonlinear equations are not always exactly conserved in the LB models due to the higher-order corrections. For instance, for Burgers' and KdV equation, ρ^2 is a conserved density of the exact equations, but not exactly conserved by the lattice

Boltzmann model. In a previous study [6], $\int dx\ \left(-3\rho^2+\partial_x^2\rho\right)$ is attempted to be conserved in ϵ^0 order with a proper choice of initial conditions. Although we don't pursue that approach in this work, we find ρ^2 is conserved well in the latter tests.

Let us summarize and compare features of the Chapman-Enskog (CE) method and the Taylor expansion (TE) methods. The two methods are similar in that

(S1) Neighboring quantities in discrete time and space are treated by the Taylor expansion.
(S2) Higher derivative terms are less important. In the CE method this is because higher derivative terms are accompanied by higher powers of ϵ.

The two methods are different in that

(D1) Order matching is necessary for the CE method, but not for the TE method.
(D2) Time ordering is used for the CE method, but not for the TE method.
(D3) In the TE method, we must assume at the outset that $\tau > 1/2$. This assumption is never explicitly required in the CE method.
(D4) The form of the equilibrium distribution is more general in the CE method.
(D5) The relation between different orders is not explicitly defined in the CE method, and this complicates the error analysis.
(D6) There exists freedom to choose the non-dimensional scalar ϵ in the CE method, but not in the TE method.

3. Numerical tests of the model

The lattice Boltzmann models proposed in the previous section were tested numerically for all three of the Burgers', KdV, and KS equations. The results were analyzed and compared with analytic solutions and solutions from previous studies, and these results are presented in the subsections below.

3.1. Model tests on the Burgers' equation

With the following boundary conditions and initial condition,

$$\rho\left(X_M,t\right) = 0, \tag{39}$$
$$\rho\left(X_m,t\right) = 2, \tag{40}$$
$$\rho\left(X,0\right) = 1-\ \tanh\left(\frac{X}{2}\right), \tag{41}$$

where X_M and X_m are the maximum and minimum X coordinates of the domain, respectively, there exists an analytic solution for Burgers' equation, Eq. (1), namely

$$\rho\left(X,T\right) = 1-\ \tanh\left(\frac{X-T}{2}\right). \tag{42}$$

We employ the D1Q5 lattice. The spatial domain used is $X\in[-10,20]$. In the first case, the scaling defined in Eq. (36) is taken to be $\alpha=\Delta X=0.1$ and $\beta=\Delta T=1.0e-3$. This means that 300 grid points are used to discretize the spatial domain.

In Fig. 1, results with $\tau=1.25$ and $\tau=1.50$ are presented. For any T and τ, there is no discernable deviation from the analytic solution. Using the scheme described in the last section, stable solutions are obtained for $0.64\leq\tau$.

Next, we tested various values for ΔX and ΔT. In Fig. 2, for each value of τ used, the ΔX- and ΔT-dependence of the global relative error,

$$G=\frac{\sum_x\left|\rho^N\left(x\right)-\rho^A\left(x\right)\right|}{\sum_x\rho^A\left(x\right)}, \tag{43}$$

are shown, where ρ^N is the numerical density and ρ^A is the corresponding analytical result. Taking into account the scaling, we found that the leading terms of the truncation error in Eq. (32) are proportional to the following terms

$$\mathcal{K}'\frac{\alpha^6}{\beta}\frac{\partial^6\rho}{\partial X^6}\propto\alpha^4\frac{\partial^6\rho}{\partial X^6},\quad \mathcal{J}'\alpha\frac{\partial^2\rho}{\partial T\partial X}\propto\beta\frac{\partial^2\rho}{\partial T\partial X},\quad \beta\frac{\partial^2\rho}{\partial T^2}, \tag{44}$$

where $\mathcal{K}'/\mathcal{J}'$ has the same form as $\mathcal{K}/\mathcal{J}$, except for its coefficient. As a result the convergence is valid to fourth order in the spatial discretization, and to first order in the time discretization.

In Fig. 2, for each value of τ considered, G at $T = 1$ is plotted against ΔX and ΔT, and fitted by a quartic and linear function, respectively. The quartic functions approach $G = 0$ as $\Delta X \to 0$. The numerical results fall on those curves and lines, respectively, demonstrating agreement with the expected order of convergence in space and time.

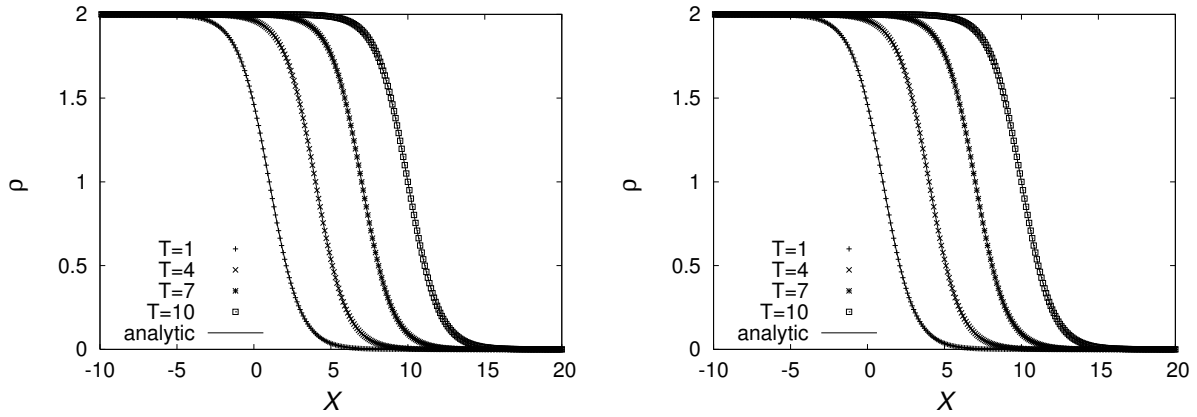

Figure 1: **Burgers' equation:** Comparison between numeric (points) and analytic (solid line) solutions when $\tau = 1.25$ (left) and $\tau = 1.50$ (right). Here we took $\Delta T = 1.0e-3$, $\Delta X = 0.1$.

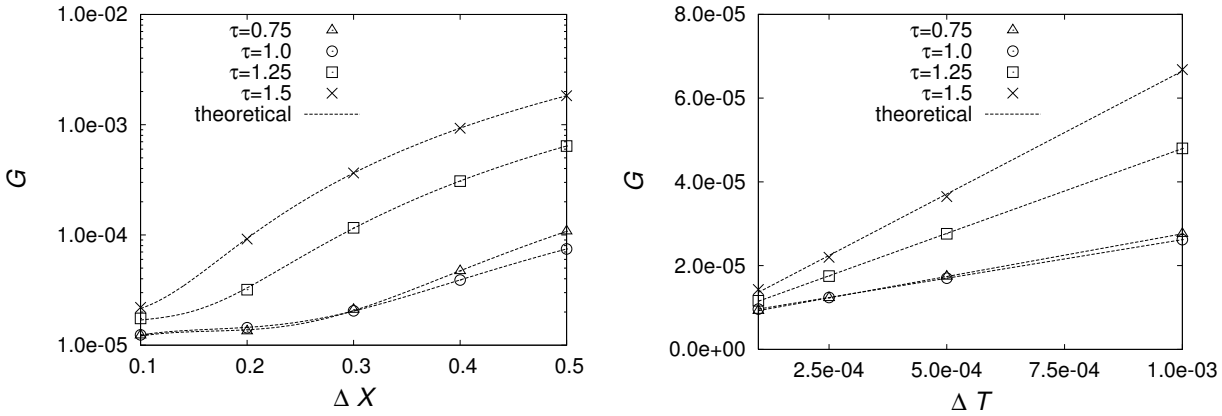

Figure 2: **Burgers' equation:** Global relative error G for $T = 1$ as a function of ΔX (left) and of ΔT (right) for various values of τ. Here we took $\Delta T = 2.5e-4$ in the left figure, and $\Delta X = 0.1$ in the right figure. The dotted quartic curves (left) and lines (right) are fits to the numeric results.

3.2. Model tests on the Korteweg-de Vries equation

In an infinite domain, with the initial condition,

$$\rho(X, 0) = -6\,\mathrm{sech}^2 X, \tag{45}$$

there exists an analytic two-soliton solution of the KdV equation, Eq. (2), namely

$$\rho(X, T) = -12\,\frac{3 + 4\cosh(2X - 8T) + \cosh(4X - 64T)}{\left[3\cosh(X - 28T) + \cosh(3X - 36T)\right]^2}. \tag{46}$$

We employ the D1Q7 lattice. The spatial domain used is $X \in [-10, 20]$ with periodic boundary conditions. In the first case, the scaling defined in Eq. (36) is $\alpha = \Delta X = 0.05$ and $\beta = \Delta T = 2.5e-6$. This means that 600 grid points are used to discretize the spatial domain.

Since the KdV equation doesn't have an explicit diffusion term, truncation error easily induces instability. Specifically, the following term, which is derived from the error terms regarding $\partial^2\rho/\partial t^2$ and $\partial^4\rho/\partial t\partial x^3$ in Eq. (32) using the KdV equation, Eq. (2), is prone to instability and growth as an unstable mode,

$$\left\{\frac{\beta\left(\mathcal{T}_2+1\right)}{2\left(\mathcal{T}_1+1\right)}-\frac{\alpha^3\mathcal{L}\left(\mathcal{T}_3+1\right)}{6\left(\mathcal{T}_1+1\right)}\right\}\frac{\partial^6\rho}{\partial x^6}:=\mathcal{G}\frac{\partial^6\rho}{\partial x^6}. \tag{47}$$

To mitigate this growth mode, the equilibrium distribution, Eq. (28), is modified by adding a term $\rho w_i^{(5)}$, where

$$\begin{aligned} w_i^{(5)} &= \mathcal{H}\left\{-\frac{5}{18},+\frac{1}{48},-\frac{1}{120},+\frac{1}{720}\right\}, \\ \mathcal{H} &= -\frac{\mathcal{G}}{\left[\alpha^6\left(\mathcal{T}_6+1\right)/\left(6!\beta\left(\mathcal{T}_1+1\right)\right)\right]}, \end{aligned} \tag{48}$$

is added, where the convention of listing lattice vectors was described in Subsection 2.3.

In Fig. 3 results with $\tau=1.00$ and $\tau=1.25$ are presented. It shows remarkable agreement with the analytic solution for both values of τ. The KdV equation is well known to possess an infinity of conserved quantities, but it would be unrealistic to expect any numerical scheme to respect all of them. The first two nontrivial conserved quantities of the KdV equation, ρ^2 and $-2\rho^3-\rho_x^2$, were observed to vary by 0.47% and 6.0% respectively during $0.1\le T\le 1$, for $\tau=1$. The algorithm was observed to be stable for $0.99\le\tau\le 20$.

Tests with different ΔX and ΔT were carried out. In Fig. 4, the global relative error G at $T=1$ is plotted versus ΔX and ΔT. For this model, we expect the main truncation error terms to be

$$\mathcal{L}'\frac{\alpha^5}{\beta}\frac{\partial^5\rho}{\partial X^5}\propto\alpha^2\frac{\partial^5\rho}{\partial X^5},\quad \mathcal{J}''\alpha\frac{\partial^2\rho}{\partial T\partial X}\propto\beta\frac{\partial^2\rho}{\partial T\partial X},\quad \beta\frac{\partial^2\rho}{\partial T^2}. \tag{49}$$

Again, $\mathcal{L}'/\mathcal{J}''$ has the same form as $\mathcal{L}/\mathcal{J}$ except for its coefficient. The convergence order is therefore expected to be second-order for the spatial discretization and first-order for the time discretization. In Fig. 4, the error is fitted to quadratic (left) and linear (right) functions, indicating results that are consistent with this expectation. Again, the quadratic curves approach $G=0$ as $\Delta X\to 0$.

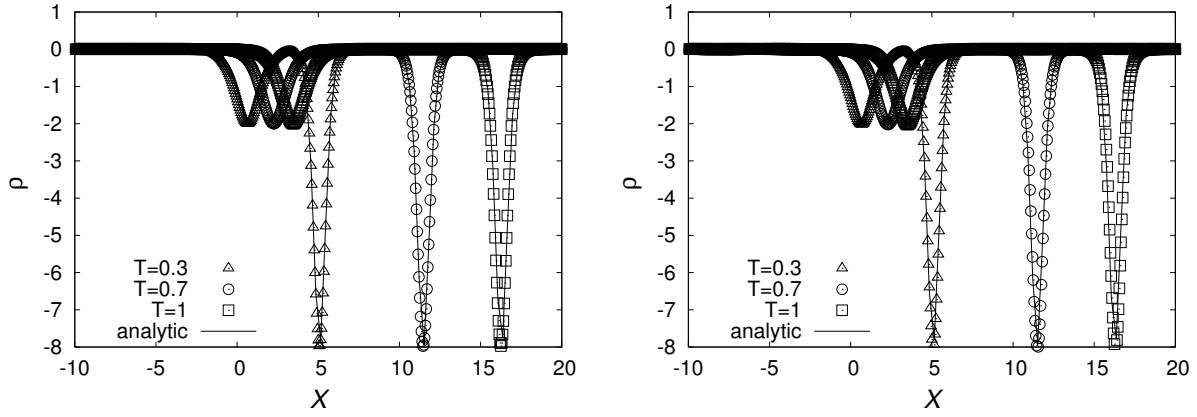

Figure 3: **Korteweg-de Vries equation:** Comparison with the analytic solution (solid line) in the case of $\tau=1.00$ (left) and $\tau=1.25$ (right). Here we took $\Delta T=2.5e-6$, and $\Delta X=0.05$.

3.3. Model tests on the Kuramoto-Sivashinsky equation

With following boundary conditions and initial condition,

$$\rho\left(X_m,t\right) = b-\frac{30}{19}\sqrt{\frac{11}{19}}, \tag{50}$$

$$\rho\left(X_M,t\right) = 2b-\rho\left(X_m,t\right), \tag{51}$$

$$\rho\left(X,0\right) = b+\frac{15}{19}\sqrt{\frac{11}{19}}\left\{-9\tanh\left[k\left(X-X_0\right)\right]+11\tanh^3\left[k\left(X-X_0\right)\right]\right\}, \tag{52}$$

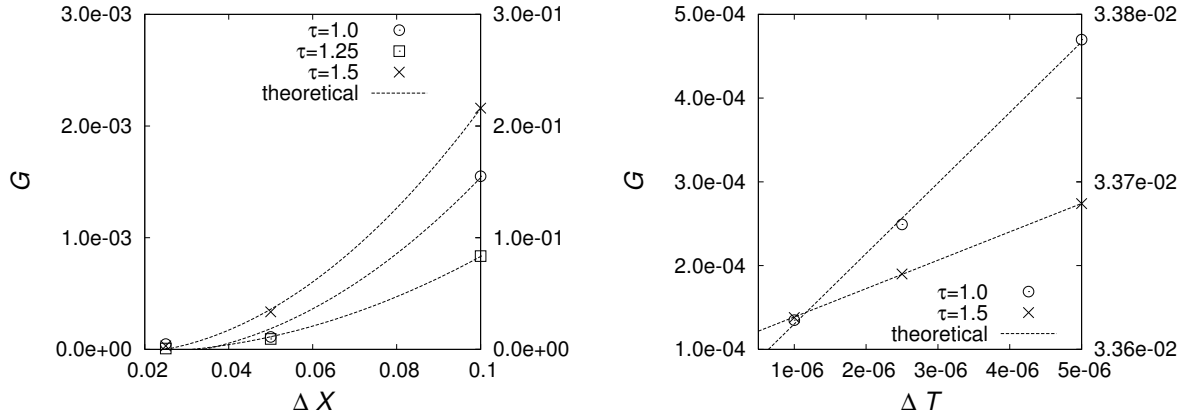

Figure 4: **Korteweg-de Vries equation:** Global relative error for $T = 1$ as a function of ΔX (left) and of ΔT (right) for various values of τ. Here we took $\Delta T = 5.0e-7$ in the left figure, and $\Delta X = 0.05$ in the right figure. In both figures, the left-hand ticks on the ordinate are for $\tau = 1$, and the right-hand ones are for the other two values of τ. The dotted quadratic curves (left) and lines (right) are fits to the numeric results.

where X_M and X_m are the maximum and minimum X coordinates of the domain, respectively, and where $k = \frac{1}{2}\sqrt{\frac{11}{19}}$, there exists an analytic solution for the KS equation, Eq. (3), namely

$$\rho\left(X,t\right) = b + \frac{15}{19}\sqrt{\frac{11}{19}}\left\{-9\,\tanh\left[k\left(X - bt - X_0\right)\right] + 11\,\tanh^3\left[k\left(X - bt - X_0\right)\right]\right\}. \tag{53}$$

We employ the D1Q5 lattice. Here $b = 3$ and $X_0 = \left(X_M - X_m\right)/3$. The spatial domain size is $X \in [-30, 30]$. In the first case, the scaling defined in Eq. (36) is $\alpha = \Delta X = 0.1$ and $\beta = \Delta T = 1.0e-5$. This means that 600 grid points are used to discretize the spatial domain.

In Fig. 5, results with $\tau = 1.25$ and $\tau = 1.50$ are presented. Once again, they indicate remarkable agreement between the numerical results and the analytic solution, and there is no obvious τ dependence. The algorithm was observed to be stable for $1.0 \leq \tau \leq 5.0$.

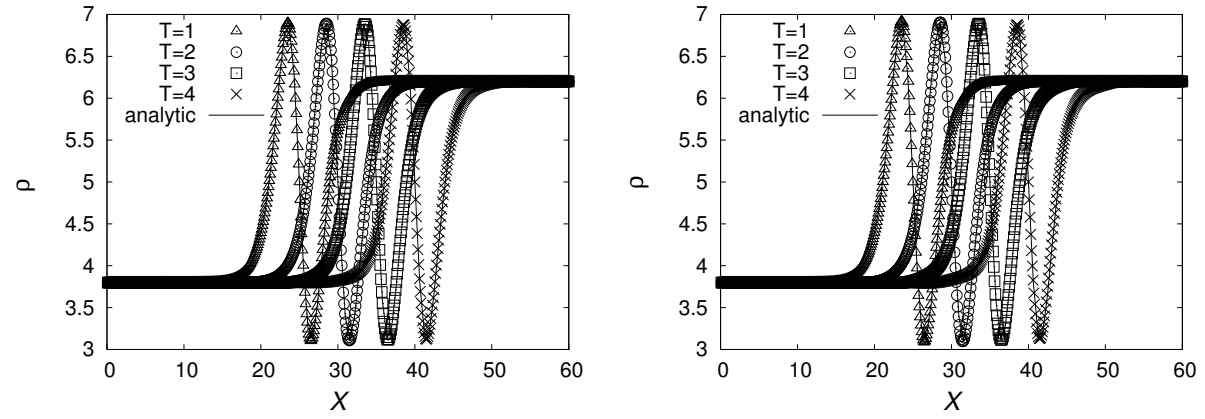

Figure 5: **Kuramoto-Sivashinsky equation:** Comparison with the analytic solution (solid line) in the case of $\tau = 1.25$ (left) and $\tau = 1.50$ (right). Here we took $\Delta T = 1.e-5$,$\Delta X = 0.1$.

Taking into account the scaling, we found that the leading terms of the trunction error in Eq (32) are proportional to the following terms

$$\mathcal{M}'\frac{\alpha^6}{\beta}\frac{\partial^6\rho}{\partial X^6} \propto \alpha^2\frac{\partial^6\rho}{\partial X^6}, \quad \mathcal{J}'\alpha\frac{\partial^2\rho}{\partial T\partial X} \propto \beta\frac{\partial^2\rho}{\partial T\partial X}, \quad \beta\frac{\partial\rho}{\partial T^2}, \tag{54}$$

where $\mathcal{M}'$ has the same form as $\mathcal{M}$, except for its coefficient. The convergence order is therefore expected to be second-order for the spatial discretization and first-order for the time discretization.

In Fig. 6, G at $T = 1$ is plotted versus ΔX and ΔT for various values of τ. The dependence on ΔX was fit to a quadratic (left) and that on ΔT was fit to a line (right). Once again, the quadratic function goes to zero as $\Delta X \to 0$, and once again the numerical results fall on those curves and lines, demonstrating agreement with the expected order of convergence in space and time, given by Eq. (54).

Furthermore in Fig. 6 results based on a previous study [3] are presented. When τ is close to one, it is clear that the present algorithm results in increased accuracy. We believe this is due to our retention of the exact BGK form of the collision operator, albeit with an equilibrium distribution defined to high order, as contrasted with the modification of the BGK form by an "amending function," defined in the earlier literature [3]. It seems to us that the amending function causes additional truncation error in the production and advection terms of the KS equation. When τ is not close to one, however, the truncation error of the diffusion term becomes dominant, as we discuss below, and therefore both models exhibit similar accuracy.

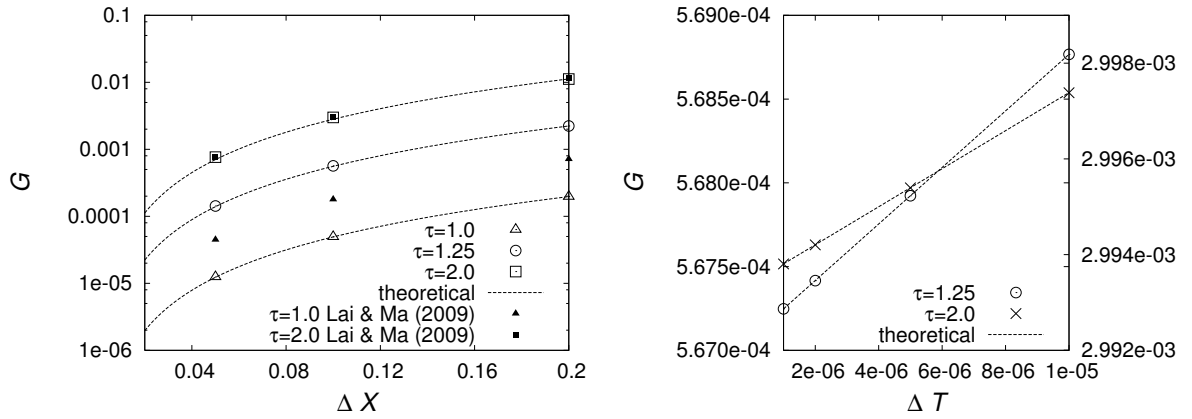

Figure 6: **Kuramoto-Sivashinsky equation:** Global relative error G at $T = 1$ as a function of ΔX (left) and of ΔT (right), for various values of τ. Here we took $\Delta T = 5.0e-7$ in the left figure and $\Delta X = 0.1$ in the right figure. In the right-hand graph, the left-hand ticks on the ordinate are for $\tau = 1.25$, and the right-hand one is for $\tau = 2.0$. The dotted quadratic curves (left) and lines (right) are fits to the numeric results.

In Fig. 7, G at $T = 1$ is plotted as a function of τ. The explicit form of the truncation error regarding the sixth-derivative terms in Eq. (32) is $Y(\Delta t, \alpha, \beta) \cdot J(\tau) \cdot \frac{\partial^6 \rho}{\partial X^6}$ where $Y(\Delta t, \alpha, \beta) = -(\Delta t)^6 \alpha^2/6$ and

$$J(\tau) = (6P_6 + 15P_5 + 20P_4 + 15P_3 + 6P_2 + P_1 + 1)/H(\tau), \tag{55}$$

$$\begin{aligned} P_1 &= \tau - 1, \\ P_2 &= \tau(\tau - 1), \\ P_3 &= \tau(\tau - 1)(2\tau - 1), \\ P_4 &= \tau(\tau - 1)\left(6\tau^2 - 6\tau + 1\right), \\ P_5 &= \tau(\tau - 1)\left(24\tau^3 - 36\tau^2 + 14\tau - 1\right), \\ P_6 &= \tau(\tau - 1)\left(120\tau^4 - 240\tau^3 + 150\tau^2 - 30\tau + 1\right), \end{aligned} \tag{56}$$

using $H(\tau)$ as defined below Eq. (31). In Fig. 7, the numerical data for G is fitted by the function $J(\tau)$. The numerical results can be made to lie on each curve using only a parameter, thus demonstrating that most of the τ-dependence of G probably comes from such a sixth-derivative term.

The above error analyses indicate that the sixth-derivative term is important for enhancing the accuracy associated with τ and ΔX dependence. Indeed it is not straightforward with a five-speed model ($Q = 5$) to remove this term because there are too few degrees of freedom in a five-speed model to control a sixth derivative. Even if this problem is addressed by using a larger stencil (more speeds), the coefficients of the higher-order terms must be carefully checked to ensure that a strongly unstable growth mode is not included.

4. Discussion and conclusions

We have compared the Chapman-Enskog method and the Taylor expansion method for the derivation of non-linear hydrodynamic equations from the LB equation. The reader will recall that features of

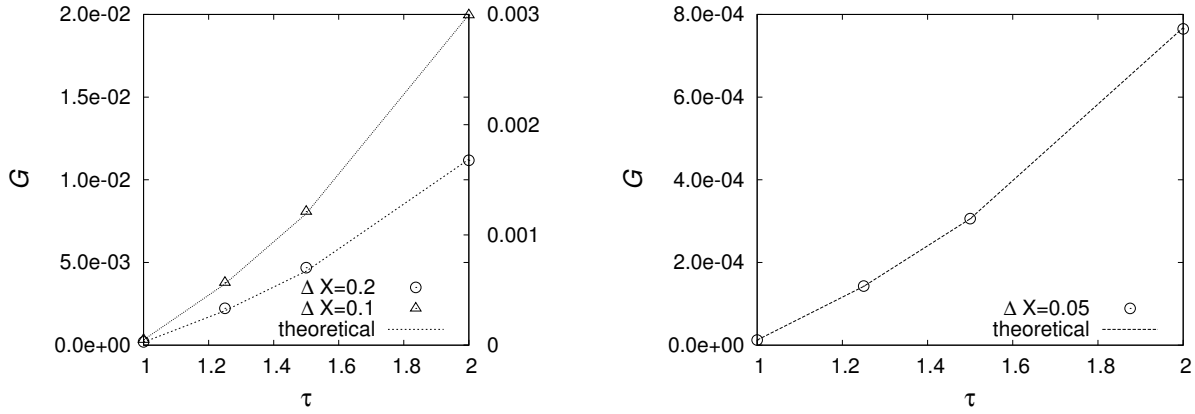

Figure 7: **Kuramoto-Sivashinsky equation:** Global relative error G at $T = 1$ as a function of τ with various lattice resolutions. Here we took $\Delta T = 5.0e-7$. In the left-hand figure, the ordinate ticks on the left are for $\Delta X = 0.1$ and those on the right are for $\Delta X = 0.2$. Each plot is fitted by $J(\tau)$, defined in Eq. (55).

the two methods were compared and contrasted in Subsection 2.3. From those observations, we would propose that, when LB models for nonlinear hydrodynamic equations are derived, it is best to start with the Chapman-Enskog method using the general equilibrium state. After results to leading order are obtained, the Taylor expansion method can be applied for error analysis and enhancement of stability and accuracy.

In this work, we derived LB models for the Burgers', KdV, and KS equations using a single consistent theoretical framework, and we compared numerical results from each of those models to corresponding analytic results, demonstrating remarkable accuracy. Error scaling in ΔX, ΔT and τ was shown to be in agreement with theory. Numerical stability over a wide range of τ was also demonstrated. For our LB models for the KS equation, our quantitative results were compared with a previous study [3], and shown to have enhanced accuracy, especially in the vicinity of $\tau = 1$.

In future work, in order to enhance accuracy and stability for the time discretization, higher-order time-marching methods such as Adams-Moulton and Adams-Bashforth could be applied. In addition, although the LB models presented in this work were formulated so that any τ reproduces the same hydrodynamic equation to leading order, the application of the method to more general equations that have different coefficients could be formulated so that varying τ yields hydrodynamic equations with the desired coefficients. Alternatively one could employ the multiple-relaxation-time (MRT) LB methodology to increase the number of degrees of freedom in the model.

In closing, from the experience we gained in deriving and simulating these models, we would argue that the LB method has certain particular virtues for the simulation of nonlinear systems of this sort. For example, the LB methodology is capable of modeling non-linear hydrodynamic equations conserving ρ from a LB equation using one consistent theoretical framework. By adjusting the manner of particle propagation and the collision process, it can be applied to a wide variety of such systems. Moreover, at least for the systems considered in this paper, the nonlinearity of the associated LB models is isolated in the collision operator which is purely local. This feature allows for highly efficient parallel computer implementation.

Acknowledgements

This work was supported by a French public grant as part of the Investissement d'avenir project, reference ANR-11-LABX-0056-LMH, LabEx LMH. Two of us (BMB and FD) would like to thank the Fondation Mathématique Jacques Hadamard (FMJH) for travel funding that made this collaboration possible.

[1] S.Succi, The Lattice Boltzmann Equation for Fluid Dynamics and Beyond, first ed., Oxford University Press, Oxford, 2001

[2] L.Ye, G.Yan, T.Li, Numerical method based on the lattice Boltzmann model for the Kuramoto-Sivashinsky equation, J.Sci.Comput. 49 (2011)195-210

[3] H.Lai, C.Ma, Lattice boltzmann method for the generalized Kuramoto-Sivashinsky equation, Physica A. 388(2009)1405-1412

[4] B.Shi, N.He, Z.Guo, Lattice boltzmann model for high-order nonlinear partial differential equations,arXiv:0907.1720

[5] C.Lin-Jie, M.Chang-Feng, A lattice Boltzmann model with an amending function for simulating nonlinear partial differential equations, Chin.Phys.B 19(2010)010504

[6] J.Zhang, G.Yan, A lattice Boltzmann model for the Korteweg-de Vries equation with two conservation laws, Comput.Phys.Commun 180(2009)1054-1062

[7] G.Yan, J.Zhang, A higher-order moment method of the lattice Boltzmann model for Korteweg-de Vries equation, Math.Comput.Simulat 79(2009)1554-1565

[8] D.J.Holdych, D.R.Noble, J.G.Georiadis, R.O.Buckius, Truncation error analysis of lattice Boltzmann methods, J.Comput.Phys. 193 (2004)595-619

[9] A.J.Wagner, Thermodynamic consistency of liquid-gas lattice Boltzmann simulations, Phys.Rev.E. 74 (2006)056703

[10] F.Dubois, Equivalent partial differential equations of a lattice Boltzmann scheme, Comput.Math.Appl. 55 (2008)1441-1449

[11] D.Lycett-Brown and K.H.Luo, Improved forcing scheme in pseudopotential lattice Boltzmann method for multiphase flow at arbitrarily high density ratios, Phys.Rev.E. 91 (2015)023305

[12] G.Sivashinsky, D.Michelson, On irregular wavy flow of a liquid film down a vertical plane, Progr.Theoret.Phys. 63 (1980)21122114

[13] S.Sharafatmandjoor, N.A.C.Sidik, F.Sabetghadam, Analysis of the applicability of the lattice Boltmann method in targeting a chaotic flame front model, Numer.Heat.Transfer.partA. 67 (2015)597-603

[14] G.Sivashinsky, Nonlinear analysis of hydrodynamic instability in laminar flames I. Derivation of basic equations, Acta.Astron. 4 (1977)11771206

[15] P.Holmes, J.Lumley, G.Berkooz, C.W.Rowley, Turbulence, coherent structures, dynamical systems and symmetry, Cambridge university press, Cambridge, 2012

[16] Y.H.Qian, Y.Zhou, Higher-order dynamics in lattice-based models using Chapman-Enskog method, Phys.Rev.E. 61 (2000) 2103